Science of the Total Environment 868 (2023) 161666

Contents lists available at ScienceDirect

Science of the Total Environment

journal homepage: www.elsevier.com/locate/scitotenv

A desiccated dual-species subaerial biofilm reprograms its metabolism and affects water dynamics in limestone

F. Villa [a,*,1], N. Ludwig [b,1], S. Mazzini [a], L. Scaglioni [a], A.L. Fuchs [c,2], B. Tripet [c], V. Copié [c], P.S. Stewart [d], F. Cappitelli [a]

[a] Dipartimento di Scienze per gli Alimenti, la Nutrizione e l'Ambiente, Università degli Studi di Milano, 20133 Milan, Italy
[b] Dipartimento di Fisica Aldo Pontremoli, Università degli Studi di Milano, 20133 Milan, Italy
[c] Department of Chemistry & Biochemistry, Montana State University, Bozeman, USA
[d] Center for Biofilm Engineering, Montana State University, Bozeman 59717, USA

HIGHLIGHTS

- Drought changes the composition, structure, and metabolic profile of a dual-species SAB while reducing oxidative stress
- SAB metabolism responds to drought stress by shifting to fermentation
- Desiccated dual-species SABs protect the stone from rapid water uptake and evaporation
- Desiccated dual-species SABs change the wetting properties of the stone.
- Desiccated dual-species SABs affect the flux of water between the substrate and the environment.

GRAPHICAL ABSTRACT

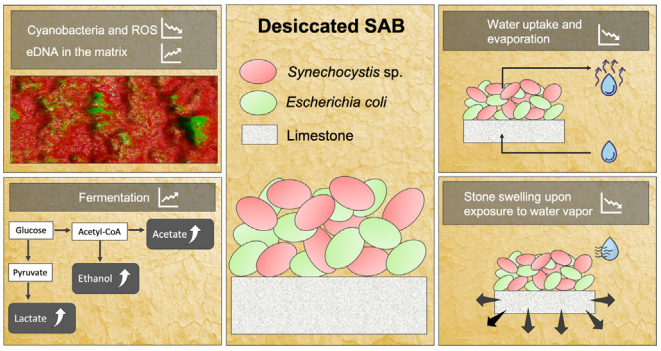

ARTICLE INFO

Guest Editor: Patricia Sanmartín

Keywords:
Drought
Desiccated subaerial biofilm
Fermentation
Water dynamic
Swelling

ABSTRACT

Understanding the impact of sessile communities on underlying materials is of paramount importance in stone conservation. Up until now, the critical role of subaerial biofilms (SABs) whether they are protective or deteriorative remains unclear, especially under desiccation. The interest in desiccated SABs is raised by the prediction of an increase in drought events in the next decades that will affect the Mediterranean regions' rich stone heritage as never before. Thus, the main goal of this research is to study the effects of desiccation on both the biofilms' eco-physiology and its impacts on the lithic substrate. To this end, we used a dual-species model system composed of a phototroph and a chemotroph to simulate biofilm behavior on stone heritage. We found that drought altered the phototroph-chemotroph balance and enriched the biofilm matrix with proteins and DNA. Desiccated SABs underwent a shift in metabolism to fermentation and a decrease in oxidative stress. Additionally, desiccated SABs changed the water-related dynamics (adsorption, evaporation, and wetting properties) in limestone. Water absorption experiments showed that desiccated SABs protected the stone from rapid water uptake, while a thermographic survey indicated a delay in water evaporation. Spilling-drop tests revealed a change in the wettability of the stone-SAB interface, which affected the water transport properties of the stone. Finally, desiccated SABs reduced stone swelling in the presence of water vapor. The biodeteriorative and bioprotective implications of desiccated SABs on the stone were ultimately assessed.

* Corresponding author.
E-mail addresses: federica.villa@unimi.it (F. Villa), nicola.ludwig@unimi.it (N. Ludwig), stefania.mazzini@unimi.it (S. Mazzini), leonardo.scaglioni@unimi.it (L. Scaglioni), brian.tripet@montana.edu (B. Tripet), vcopie@montana.edu (V. Copié), phil_s@montana.edu (P.S. Stewart), francesca.cappitelli@unimi.it (F. Cappitelli).
[1] Villa and Ludwig contributed equally to this work.
[2] Current affiliation: National Institutes of Health, National Human Genome Research Institute, Medical Genomics and Metabolic Genetics Branch, Metabolism, Infection, and Immunity Section, Bethesda, MD 20892, USA.

http://dx.doi.org/10.1016/j.scitotenv.2023.161666
Received 23 October 2022; Received in revised form 10 January 2023; Accepted 13 January 2023
Available online 18 January 2023

1. Introduction

The mineral-air interface is a large ecological niche that has existed since the dawn of Earth. Despite the stark and oligotrophic environment, the mineral-air interface hosts a thin veneer of densely packed microorganisms living within an extracellular polymeric matrix (EPM) that they produce themselves. These well-organized self-sufficient communities that colonize the mineral substrates exposed to the atmosphere are called subaerial biofilms (SABs) (Gorbushina, 2007).

SABs are not passive colonizers, but are rather dynamic ecosystems receptive to environmental changes, being sensitively tuned to both the substrate and the air. They are well adapted to extreme and fluctuating environments, which promote the development of specialized microorganisms with efficient metabolic stress responses (Villa and Cappitelli, 2019). Similar to other mineral substrates, stone monuments are an inescapable target of SAB colonization. The keystone species of SAB communities on stone monuments are oxygenic phototrophs that often cohabitate with chemoorganotrophs (Gaylarde et al., 2012). Phototrophs, such as cyanobacteria, sustain chemoorganotrophs development by providing photosynthetically fixed carbon, exudates, and cell debris (Albertano, 2012; Gaylarde et al., 2017; Gulotta et al., 2018; Sanmartín et al., 2020). Chemoorganotrophs promote phototrophs growth by consuming oxygen, supplying key metabolites, and scavenging waste products (Villa and Cappitelli, 2019).

The growth of SABs on stone heritage has long been associated with a conservation threat—namely biodeterioration—as investigated and reviewed by several researchers (inter alia Branysova et al., 2022; Liu et al., 2020; Potysz and Bartz, 2022). Biodeterioration is defined as any undesirable change in the material property caused by the activities of organisms. However, the finding of SABs on deteriorated stones does not always mean that they are responsible for the decay as is frequently thought (Favero-Longo and Viles, 2020; Liu et al., 2022). Remarkably, a growing number of studies have claimed that SABs on stones have a neutral and even a protective effect (Carter and Viles, 2005; Gulotta et al., 2018; Pinna, 2014; Sanmartín et al., 2020; Warscheid and Leisen, 2011). Some of the proposed protective mechanisms include the lowering of water level within the stone and the mitigation of the physical and chemical weathering (Bartoli et al., 2014; Cutler et al., 2013; Mottershead et al., 2003). For instance, the highly hydrophobic algal biofilm growing on the processional cloister of the Monastery of San Martiño Pinario created a hydrophobic layer that altered the original wettability of the building material, preventing the entry of water and the associated damages (Sanmartín et al., 2020). Understanding the range of impacts of sessile communities on the materials' surface would be of paramount importance for stone conservation (Naylor et al., 2002). Currently, however, the investigation on the role of SABs as being protective or deteriorative has been very limited.

The scientific evidence suggests that environmental changes will potentially alter the relationship between the SAB and the lithic substrate, with important implications for conservation strategies (Goller and Romeo, 2008; Viles and Cutler, 2012). Drought is one of the environmental conditions that affect the SAB's physiology and activity. Drought is water deficiency that drives ecosystems beyond vulnerability thresholds, impacts ecosystem services, and triggers feedback in natural and human-made systems (Crausbay et al., 2017). After all, water is one of the most essential factors for the growth of all organisms. By functioning as a temperature buffer and a solvent, water affects pH, oxygen level, hydrodynamics, osmolarity, and diffusion of ions and nutrients in the biofilm community.

Although the global climate models vary in many ways, they all agree on the prediction of increasing drought in the Mediterranean regions in the coming decades with potentially 40 % less precipitation (Tuel and Eltahir, 2020). Since drought will be a key driver in the ecological dynamics of the Mediterranean regions, hence, the regions' rich stone heritage, we studied the effects of desiccation on both the SABs' physiological response and impact on the lithic substrate. To this end, a dual-species SAB grown on limestone was used in this study based on the metabolic coupling between a phototroph and a heterotroph and simulating actual field conditions (Villa and Cappitelli, 2019). The desiccated SABs' structural and metabolic changes were investigated, along with the stones' water-related dynamics. The biodeteriorative and bioprotective implications of desiccated SABs on the stone were ultimately assessed.

2. Materials and methods

2.1. SAB growth and desiccation experiments

Dual-species SABs, composed of the phototroph *Synechocystis* sp. PCC 6803 and the heterotroph GFP-*Escherichia coli* K12 MG1655, were grown according to the protocol reported by Villa et al. (2015). The lithic substrates used in this study were commercial limestone specimens (H:75 mm × L:23 mm × T:10 mm) consisting of 90 % calcite and dolomite and with a porosity of 8.91 % ± 0.78. The limestone specimens were inoculated with the phototroph-heterotroph planktonic culture of approximately 5×10^7 cell/mL of each microorganism, placed in a modified Drip Flow Reactor set on a surface held at a 10° slant and attached to the medium reservoir. The mineral medium BG11 (Rippka et al., 1979) was pumped through the system every 12 min at 1 mL/min for 3 min, creating a discontinuous flow rate. The reactor operated in discontinuous flow mode for 10 days at room temperature under a 14/10 day/night photoperiod and 40 μmol (photons)/(m^2 s) illumination.

After 10 days, mature dual-species SABs were divided into two groups. One group was kept hydrated with the BG11 solution, and the other group was desiccated. The desiccation was carried out by interrupting the BG11 inlet (water deficiency) and by providing an air-blast drying to induce evaporative water loss. The air-blast device was composed of the influent tube attached to the air pump set at 1 L/min (Whisper 20, Tetra), ultrafilter membranes, and rubber tubing. Air entered the reactor at the top of each channel, and exited at the bottom through the effluent port, without being pressurized in the DFR. The SABs were exposed to water deficiency and air-blast for 24 h. Both hydrated and desiccated SABs were immediately processed for further analyses.

2.2. Biomass quantification and visualization, EPM characterization and oxidative stress

The structure of the hydrated and desiccated SABs was visualized by confocal laser scanning microscopy (CLSM). Confocal images were collected using a Leica TCS-SP5 confocal microscope (Leica Microsystems Heidelberg GmbH, Germany) and a 20× dry objective. Fluorescence was excited and collected using the following laser lines and emission parameters: for GFP-tagged *E. coli* cells, ex 488 nm, em 500–550 nm, and autofluorescence of *Synechocystis* sp. with ex 633 nm, and em 650–750 nm. Captured images were analyzed with the software Imaris (Bitplane Scientific Software, Switzerland) for 3D reconstructions of SABs. A minimum of three SABs samples for each condition were analyzed and representative images were presented. The images were also processed to quantify the proportion of red and green signals in hydrated and desiccated SABs using Imaris software.

The biomass of hydrated and desiccated SABs was collected by gently scrubbing off the surface with a sterile toothbrush and placed in PBS. Viable cell counts were determined as previously reported by Villa et al. (2015). Data from colony counts were taken from three different experiments (each dilution plated in triplicate) and used to calculate the number of CFU per cm^2 for each microorganism.

The extracellular polymeric matrix (EPM) of both hydrated and desiccated SABs was characterized in terms of carbohydrates, proteins, and extracellular DNA (eDNA) content following the procedure described by Villa et al. (2012). Briefly, the EPM was extracted using the EDTA method followed by centrifugation, and filtration of the supernatant with 0.2 μm polyethersulfone membranes (S623; Whatman, Florham Park, NJ). Then, one-half of the eluate was used for the quantification of proteins and carbohydrates according to the Bradford and the phenol–sulfuric acid

methods, respectively. The second half of the eluate was used for the extracellular DNA (eDNA) quantification based on the (CTAB)-DNA method. Results were normalized by the CFU/cm^2. Experiments were performed in triplicate.

The level of oxidative stress in hydrated and desiccated SABs was determined by using 2′,7′-dichlorofluorescein diacetate assay according to (Jakubowski et al., 2000). The fluorescence of the supernatant was measured using the fluorometer VICTOR™ X Multilabel Plate Readers (Perkin Elmer), excitation 490 nm, and emission 519 nm. The emission values were normalized by the CFU/cm^2. Experiments were conducted in triplicate.

2.3. Metabolites extraction and detection

Polar metabolites were extracted for NMR metabolomics similar to what has previously been reported (Fuchs et al., 2016). Briefly, hydrated and desiccated SABs were collected by gently scrubbing off the surface with a sterile toothbrush and placed in 5 mL of PBS. The resulting suspensions were centrifuged at 5000 rpm for 10 min at 4 °C. Cell pellets were resuspended in 1.5 mL of 50 % aqueous methanol and placed at −80 °C for a minimum of 2 h to allow for the solution to freeze. Cells were subsequently thawed and transferred to glass tubes, followed by sonication for 30 s. The freeze-thaw cycle was repeated twice, followed by centrifugation at 14,000 ×*g* for 5 min at 4 °C, and resulting supernatants were transferred to new microcentrifuge tubes. An equivalent volume of chloroform was added to the supernatant and thorough mixing was achieved by briefly vortexing the suspension. Subsequent phase separation was achieved by centrifugation at 14,000 ×*g* for 5 min at 4 °C. Following this step, the top aqueous methanol phase was transferred to a separate tube and dried using a speed vacuum instrument overnight with no heat. The resulting dried metabolite mixtures were stored at −20 °C until further analysis by NMR. Dried intracellular metabolite extracts were resuspended in 700 μL of NMR buffer (25 mM NaH_2PO_4/Na_2HPO_4, 0.4 mM imidazole, 0.25 mM DSS, 100 % D_2O, pH 7), followed by a quick centrifugation step to remove any insoluble material, and transferred to 5 mm Wilmad NMR tubes, as described in Fuchs et al. (2016). NMR samples were prepared from triplicate experiments with duplicate technical replicates for each condition.

2.4. NMR data acquisition and processing

1D ^{1}H NMR spectra were recorded at 298 K (25 °C) using a Bruker AVANCE III 600 MHz (^{1}H Larmor frequency) solution NMR spectrometer equipped with a 5 mm triple resonance (^{1}H, ^{15}N, ^{13}C) helium-cooled TCI cryoprobe, a SampleJet automatic loading system, and Topspin software (Bruker version 3.2). 1D ^{1}H NMR data acquisition was performed using the Bruker-supplied 'noesypr1d' pulse sequence, and NMR spectra were recorded using a ^{1}H spectral window of 9600 Hz and 256 scans. FIDs were collected using 32 K data points and a dwell time interval of 52 ms, amounting to a data acquisition time of 1.7 s. The relaxation recovery delay was set to 2 s with a mixing time period of 50 msec between scans. DSS was used for chemical shift referencing and relative intensity calibration, while the imidazole signal was used to correct for slight chemical shift changes due to small pH discrepancies between samples. Chemical shift referencing and spectra preprocessing including baseline correction, zero filling, and phasing were done using Topspin. Further processing of 1D NMR spectra including identification and quantification of metabolites was conducted using the Chenomx software (version 8.0). Further validation of metabolite IDs was done using 2D NMR, including 2D ^{1}H—^{1}H TOCSY experiments as described in Fuchs et al. (2019).

Metabolite concentrations (mM) obtained from the profiling of metabolites using Chenomx were exported and converted to attomoles per CFU by accounting for NMR volumes and normalizing metabolite levels to CFU. For univariate and multivariate statistical analysis using the MetaboAnalyst software (version 3.0) (Xia et al., 2015), metabolite concentrations were further log (base 2) transformed to ensure a Gaussian distribution of the data and auto-scaled (i.e., mean-centered and divided by the standard deviation). Metabolites with a false discovery rate (FDR) corrected *p*-value less or equal to 0.05 were considered significant. Student's *t*-test, PCA, and PLS-DA were conducted to assess similarities and differences in metabolite profiles between hydrated versus desiccated sample groups. Variable of importance in projection (VIP) plots were used to assess the contribution of specific metabolites to the group separations observed in the PLS-DA model. Metabolites with VIP scores > 1 were considered significant.

2.5. Magnetic resonance imaging (MRI)

Stone specimens without and with SABs under different water regimes (hydrated vs. dehydrated SABs) were cut into a cube to fit snugly into the 10-mm diameter NMR tubes. The uncolonized surface, opposite to the colonized surface, was in contact with water. The NMR tubes were then subjected to vacuum for 110 s. Water absorption under vacuum guaranteed air removal inside the pores and then water penetration into the pores from the bottom of the stone. The images were acquired at 25 °C using a standard bore Bruker Avance AV600 spectrometer, operating at ^{1}H resonance frequency of 600.13 MHz, equipped with a 10 mm ^{1}H micro-imaging probe and a variable temperature control unit. The MRI signal intensity is correlated to the quantity of water in the stone. Bright regions in these MRI images reveal the presence of water inside the stone pores, where each pixel is proportional to the water amount in the corresponding voxel. The image data from the native format were converted into a numerical format suitable for quantitative analysis. Image analysis and data processing were performed with ParaVision v. 4.0. The software shows the map of the water signal intensities of a region of interest (ROI), selected by the user. Given an ROI binary mask image, the software extracts values and reports the mean and variance that can be analyzed. Using XLSTAT (Addinsoft, version 2022.2.1), a three-parameter asymptotic regression model was fitted to the experimental data to predict the water saturation value in the stones without and with SABs. Experiments were conducted in triplicates.

2.6. Capillary water absorption coefficient (A_{cap})

The capillary water absorption coefficient of stones without and with desiccated SABs was based on upwards suction combined with the weighing method adapted from UNI EN 1925:2000. Stone specimens were first dried in an oven at 104 °C to a constant weight, and then all surfaces, except the test surface with the SAB, were sealed with the moisture-barrier parafilm to ensure one-directional transport of water. After the sealing, the specimen was placed with the test surface facing down on a support frame in a water tank at a temperature of 20 ± 1 °C. During the test, the water level was maintained at 5 mm above the bottom of the specimen, and the specimen was removed every 15 s. The surface moisture was removed with a damp pad and the specimen was weighed immediately. The experiments last till the water content in the sample reaches an asymptotic value. All the gravimetric measurements were carried out with a Mettler Toledo balance (10^{-4} g precision). The means of cumulative water inflow per unit area (kg/m^2) were plotted against the square root of time (s$^{1/2}$) during the first 3 h. The angular coefficients of the linear trend of the curves determined the A_{cap} values.

2.7. Thermographic analyses and evaporation flux (Φ)

A thermal camera (AVIO R500EX-pro, uncooled microbolometric detector, 640 × 480 pixels) was used to monitor over time the evaporation process of limestone specimens without and with SABs under desiccation. The thermal camera was mounted on the roof of a climatic chamber (Piardi, Italy) set at 25 °C and 50 % relative humidity. The samples, after being saturated by immersion, were sealed as described in 2.6 in order to leave only the colonized surface free to evaporate. Then, samples were placed inside the climatic chamber until the limestone specimens (without and with SAB) reached the moisture equilibrium with the environment. In our case, this occurred after about 5 h for the SAB-free control samples. Experiments were conducted in triplicates.

In addition, the evaporation flux (Φ)—the flux of water vapor mass that leaves the surface of the stone expressed in kilogram per unit of surface per

unit of time—was determined. The values were obtained from the continuous weight measurements of the samples placed in the climatic chamber with a precision balance (Mettler Toledo balance, 10^{-4} g precision). Evaporation fluxes (kg/(m^2 s)) were plotted versus the water content of the samples, defined as the water mass contained in the sample with respect to the weight of the dried sample (oven 104 °C for 24 h).

2.8. Spilling drop test and UV fluorescence

The spilling drop test evaluates the wettability of a surface by using a thermal camera to study how far a drop of water spreads over a stone surface after its deposition (Ludwig et al., 2018). During 30 s of shooting, one drop of distilled water (0.03 mL) was spilled on top of stones without and with desiccated SABs. Thermal images were acquired to show the drop spreading on the surface according to the physical features of the material (e.g., hydrophobicity, porosity, roughness) (Rosina et al., 2008). The cold area of the deposited drop was evaluated by proper segmentation software that counts the number of pixels below a certain temperature threshold (Melada et al., 2020a,b). UV fluorescence was used to single out the area where desiccated SABs were present since the visible light induced by the UV lamp fluorescence provides evidence of biological materials on stones. Experiments were conducted in triplicates.

2.9. In-vivo rehydration experiments

Desiccated SABs were inserted into an environmental chamber (Pathology Devices LiveCell+ system, USA) to control both the temperature and the humidity. The chamber was mounted on the motorized stage of an inverted Leica TCS SP5 confocal microscope (Leica Microsystems Heidelberg GmbH, Germany). The CLSM control software was set to take a series of time-lapse xyzt scans at intervals of 5 min at different depths in the biofilm over a period of 90 min. The environmental chamber was set at 25 °C, and the relative humidity (RH) was gradually increased from 28 % to 90 %. This wide range includes daily changes in RH: low around midday, rapid increase in the late afternoon and early evening, and peaking at midnight. Biofilms were scanned at 600 Hz using a 10× dry objective with 488 nm and 633 nm laser excitation lines to visualize both green GFP-*E. coli* cells and the red autofluorescence of the phototrophic component of the dual-species SAB. In addition, the CLSM was used in reflectance mode with the 488 nm argon line for relief imaging of specimens. Images were analyzed in MetaMorph software (Universal Imaging Corp., Downingtown, PA) in order to estimate the vertical swelling of the stone substrate and to track the average fluorescence intensity of the entire image for each channel. Average intensity values were normalized by dividing the fluorescence intensity recorded at the different time points by the initial average fluorescence intensity values. Experiments were conducted in triplicates.

3. Results and discussion

3.1. Drought changes the composition, structure and metabolic profile of SABs while reducing oxidative stress

Periodic water deficiency that pushes the ecosystems beyond their vulnerability threshold will become more frequent in the near future. Thus, an extreme drought intensification arising from climate change raises concerns about how the stone ecosystem—composed of the SAB and the lithic substrate—responds to such events. The mechanisms of desiccation tolerance in many microorganisms isolated from different SABs have been extensively studied for decades (Bar-Eyal et al., 2015; Potts, 1999; Raanan et al., 2016). Although these studies were instrumental to understanding

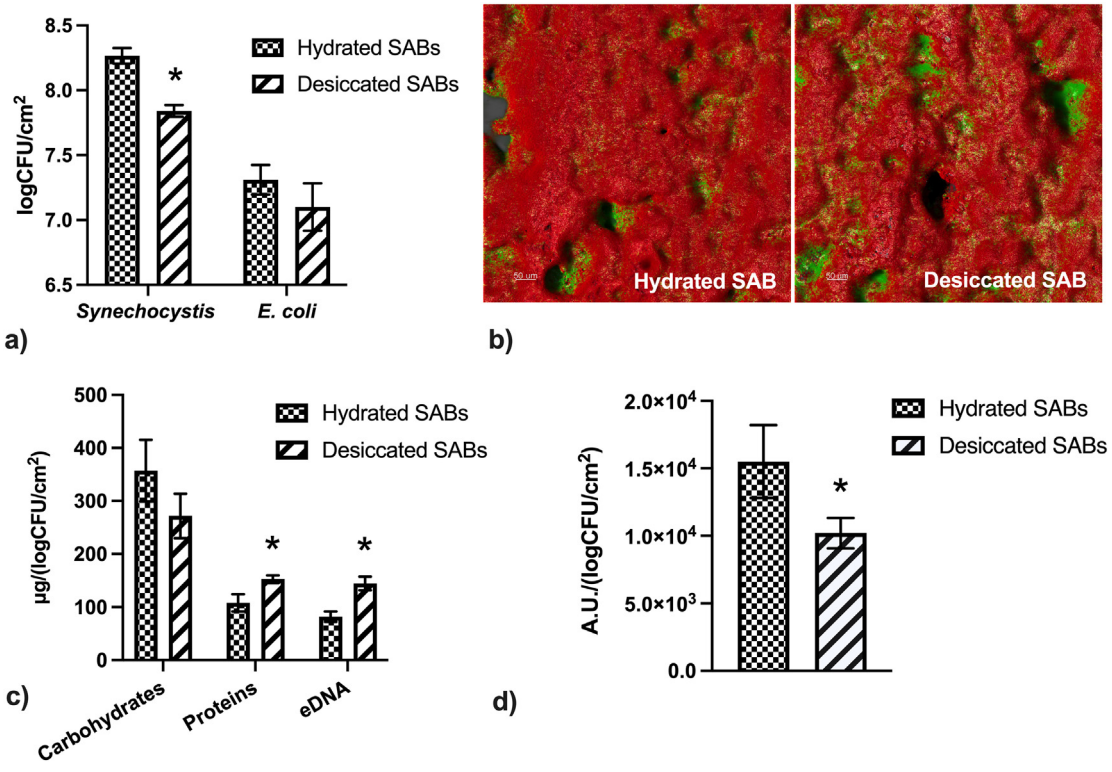

Fig. 1. Panel (a) shows the composition of hydrated and desiccated dual-species SABs measured as viable cells count. Colony-forming units (CFU) are normalized by the surface area (cm^2). Panel (b) displays the 3D reconstruction of cell aggregates in hydrated and desiccated SABs. Color key: *E. coli* cells, green (GFP); *Synechocystis* cells, red (autofluorescence). The bars in the CLSM images represent 50 μm. Panel (c) displays the biochemical composition of the EPM in the hydrated and desiccated dual-species SABs. The μg of carbohydrates, proteins and eDNA have been normalized by the number of biofilm-dwelling cells (LogCFU/cm^2). Panel (d) reports the oxidative stress experienced by the hydrated and desiccated dual-species SABs. The relative fluorescence (arbitrary unit, A.U.) has been normalized by the number of biofilm-dwelling cells (LogCFU/cm^2). Data represent the mean ± standard deviation of three independent measurements. The asterisk above the columns indicates a significant difference between the two data sets (*t*-test $p \leq 0.05$).

the structural and functional adaptations of planktonic cells to drought, they did not investigate the response of microorganisms in the biofilm state. In this paper, the eco-physiological response of a dual-species SAB to desiccation was investigated for the first time, along with its impacts on the stones' water-related dynamics.

We used well-controlled laboratory experiments with replicable dual-species SABs that resembled the phototroph-heterotroph interactions on lithic substrates (Villa et al., 2015).

Traditionally, microbial research focuses on a single species, because biofilms of a single species greatly facilitate genetic and physiology microbial growth studies and biofilm development investigation (Tan et al., 2017). In reality, however, microorganisms exist as communities, and community behavior cannot be predicted by single-species studies (Elias and Banin, 2012). The dual-species SAB herein proposed was composed of the cyanobacterium *Synechocystis* sp. and the chemoheterotroph *E. coli*. These two microorganisms have been previously retrieved on mineral substrates, highlighting their occurrence in SABs at the stone/air interface (inter alia: Bastian et al., 2010; Bellinzoni et al., 2003; Davis et al., 2020; Fernandez-Cortes et al., 2011; Ikner et al., 2007; Ortega-Morales et al., 2000; Gaylarde and Gaylarde, 2004). The scientific literature reports several SAB lab-scale systems with different combinations of microorganisms (Fuentes et al., 2022; Lianou et al., 2020). However, none of them were proven to capture the typical features of SABs such as: i) microcolonies of aggregated bacteria; ii) network-like structure conforming to surface topography; iii) cooperation and cross-feeding processes between phototrophs and heterotrophs; iv) ability to change the chemical characteristic of the microhabitats; v) survivability in harsh environments; and vi) biocide tolerance. The dual-species SAB used in this study shows symbiotic interactions between the two microorganisms and underpins functional traits of biofilm inhabiting lithic substrates (Villa et al., 2015). We are aware of the limitations of a lab-scale system that cannot fully represent the complexity and heterogeneity of a natural system. The laboratory model used was not intended to miniaturize the complex field systems, but rather to simplify the nature of the system to gain a better understanding of SAB's interaction with the lithic substrate. The dual-species SAB used here has allowed data collection through rigorous laboratory experiments that would otherwise be impossible to conduct in situ on real case studies.

Drought affected the composition of SABs as shown by a statistically significant reduction in the CFU/cm^2 of only the phototrophic component (Fig. 1a), as also seconded by CLSM analysis. The 3D reconstruction of cell aggregates in hydrated SABs showed *E. coli* colonies (green signal) mantled by *Synechocystis* cells (red signal). In desiccated SABs, the colonization pattern changed, where the red signal coverage was reduced by 32 %, which corresponded to a decrease in the phototrophic component (Fig. 1b). Our findings agreed with other experiments where stream biofilms were desiccated to mimic flow intermittence and subsequent drying (Sabater et al., 2016). Timoner et al. (2012) demonstrated that in desiccated biofilms, the autotrophic biomass was decreased by as much as 80 %, while the heterotrophic biomass was only 20 %. Acuña et al. (2015) found that dry habitats impacted the autotrophic and heterotrophic processes in the stream biofilms and promoted heterotrophy. In our desiccated SABs, the cyanobacteria can be the least resistant as it is the most exposed to the environment, but the quickest to recover after rewetting. Autotrophic processes are less resistant, but still more resilient than heterotrophic processes (Acuña et al., 2015).

The EPM of desiccated SABs had considerably higher proteins and eDNA content than that of the hydrated ones, while the polysaccharides content was statistically the same (Fig. 1c). The amount of eDNA in desiccated SABs is almost double that of the hydrated ones. This is not surprising as cell lysis under stressful conditions provides a simple mechanism for releasing DNA into the extracellular environment. Recent findings suggest that eDNA is responsible for biofilm cohesion and adhesion, possibly because it binds with the matrix polysaccharides and forms strong cross-links with multivalent cations (Hu et al., 2012; Yang et al., 2022). The eDNA confers strength and compactness to the EPM and it restricts the diffusion of molecules (Campoccia et al., 2021). The matrix compactness may reduce water loss and increase resistance to environmental stresses (Hu et al., 2012). Furthermore, desiccation-tolerant microorganisms can use eDNA as a xeroprotectant as reported by García-Fontana et al. (2016). Using molecular studies, the drought-tolerant microorganisms were shown to induce the expression of genes for the production and uptake of exogenous DNA in response to dry conditions (García-Fontana et al., 2016; Palud et al., 2020). The increasing eDNA content in the EPM of desiccated SABs may supply additional nitrogen and phosphorous and/or exogenous nucleotides, and may also contribute to horizontal gene transfer through natural transformations (Ibáñez de Aldecoa et al., 2017; Pietramellara et al., 2009).

Desiccated SABs experienced less oxidative stress than the hydrated ones (Fig. 1d). It has been reported that desiccation, and, consequently, saline stress and nutrient limitation, may destabilize the balance between oxidants and antioxidants in the cells, which leads to oxidative stress (Grzyb and Skłodowska, 2022). Oxidative stress can inflict severe damage on SAB-dwelling cells because reactive oxygen species (ROS) interaction with the cellular components causes conformational changes and loss of function. Two different mechanisms can explain the reduced ROS level in desiccated SABs. First, the inhibition of photosynthesis reduced the level of oxidative stress because the photosynthetic machinery is a major source of ROS (Raanan et al., 2016). Second, when responding to an increase in ROS concentration, the desiccated SABs possibly activated various regulators that modulate the transcription of genes involved in ROS scavenging and DNA repair (Baubin et al., 2022). An increase in antioxidant enzyme synthesis is typically a response to dehydration, however, the synthesized enzymes and the extent of the synthesis vary with species (Kranner et al., 2008).

To investigate the drought-induced metabolic responses on SABs, the metabolic profiles of hydrated and desiccated biofilms were identified and quantified using 1D ^{1}H NMR. MetaboAnalyst (Chong et al., 2018; Xia et al., 2015) was used to conduct Principal Component Analysis (PCA) on the

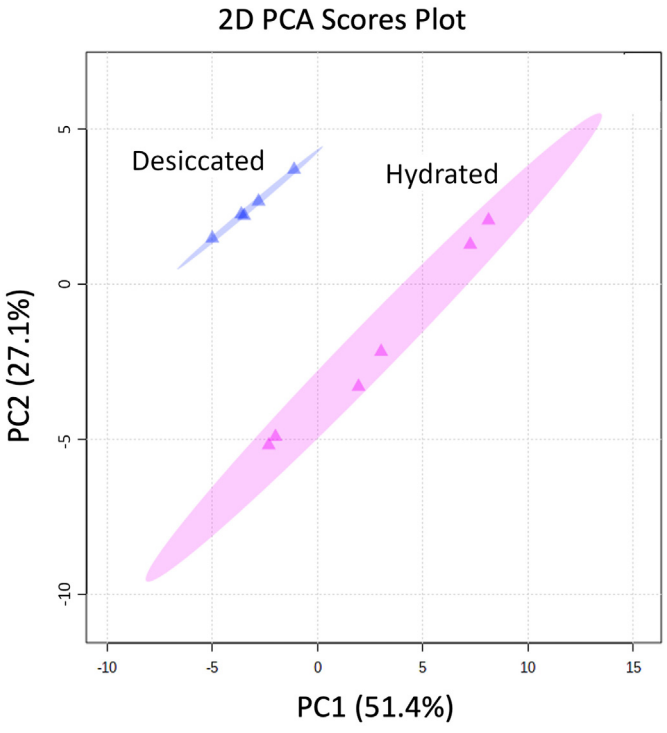

Fig. 2. Two-dimensional Principal Component Analysis (2D-PCA) scores plot generated from the multivariate statistical analysis of the intracellular metabolites profiles of hydrated (pink) and desiccated (blue) dual-species SABs. The unsupervised PCA analysis demonstrates that the intracellular metabolomes of desiccated and hydrated dual-species SABs are distinct and significantly separate the two groups, with PC 1 and PC 2 accounting together for 78.5 % of the variance. Shaded ellipses indicate 95 % confidence intervals.

Table 1
Identified intracellular and extracellular metabolites that differentiate hydrated and desiccated dual-species SABs. Concentration data are presented as mean and standard deviation (SD); ND, not detected. Metabolites are ranked according to their VIP (variable importance in projection) value. Only VIP values ≥ 1 are reported. All metabolites have a $p \leq 0.05$ where *p*-values were based on independent sample *t*-tests.

		Concentration (Attomoles/CFU)			
		Hydrated SABs		Desiccated SABs	
Metabolite	VIP	Mean	SD	Mean	SD
Cytidine	1.61	ND	ND	56.17	11.45
Formate	1.61	ND	ND	41.44	18.63
Acetate	1.49	51.41	32.95	623.96	97.87
Lactate	1.49	34.02	10.54	90.82	9.65
Guanosine	1.45	42.16	17.34	146.26	21.58
Betaine	1.39	185.33	40.51	96.72	15.33
Ethanol	1.36	19.61	13.43	1157.33	378.52
2-Hydroxy-3-methylvalerate	1.35	39.55	11.44	77.56	10.63
Aspartate	1.27	165.43	61.87	313.56	43.36
Uridine	1.27	89.38	36.22	184.38	27.19
Trehalose	1.23	66.49	26.15	30.24	4.23
Adenosine	1.20	32.10	14.39	70.88	12.83
Alanine	1.16	107.37	52.65	203.08	23.15
Acetone	1.11	2.75	0.80	4.57	1.20
Arginine	1.09	238.16	79.12	352.53	53.66
Leucine	1.06	87.46	45.43	151.97	25.56

dataset. This analysis demonstrated that the hydrated SABs were distinct from the desiccated ones (Fig. 2). PC1 and PC2 accounted for 51.4 % and 27.1 % of the overall variance, respectively, providing evidence that the dry condition changed the metabolic profile of the dual-species SABs.

To further evaluate the contribution of each metabolite to the group separation and to search for potential metabolite indicators of SABs under drought stress, variable importance in projection (VIP) scores were used to identify variables (i.e., metabolites) that have a significant impact on the SABs group separation. Metabolites whose VIP scores were greater than one (VIP > 1), were considered significant and were combined with Student's *t*-test ($p < 0.05$) to identify key metabolic markers of drought stress (Table 1).

NMR analysis of SAB metabolites identified formate, acetate, lactate, acetate, 2-hydroxy-3-methylvalerate, and ethanol as major organic acids and alcohol produced by the desiccated biofilms. These findings suggested that the SAB community performed mixed-acid fermentations for energy generation under desiccation (Fig. 3) (Stal and Moezelaar, 1997). Photosynthesis is one of the key processes affected by water deficiency. The arrest of photosynthesis during drought is a photoprotective strategy commonly observed in intertidal beach rock biofilms and biocrusts to preserve the photosynthetic machinery, guaranteeing rapid reactivation after rewetting (Thomas et al., 2022; Petrou et al., 2014). During desiccation, the photosynthetic activity of *Nostoc commune* colonies decreased with the water content and recovered rapidly upon rehydration (Sakamoto et al., 2009). Furthermore, desiccated SABs are likely to experience a decrease in O_2 availability as a result of the increased viscosity of EPM that impedes the molecular diffusion (Leprince et al., 2000). All these phenomena can promote an anaerobic environment for fermentation. After all, the onset of fermentation does not require a strict anoxic condition, but a reduced oxygen partial pressure, as demonstrated by many cyanobacteria including *Nostoc* sp. that performed fermentation with 3.4 % oxygen in the gas phase (Stal and Moezelaar, 1997). *E. coli* produced acetate, lactate, and formate during mixed-acid fermentation as well as ethanol (Vuoristo et al., 2015). Angermayr et al. (2016) suggested that *Synechocystis* sp. ferments in the dark and anoxic period, leading to intracellular acetate and lactate formation. The energy yield from the conversion of glycogen to acetate and lactate presumably covered the general costs of cellular maintenance during the anoxic period. Acetate and lactate production could also be derived from a shift toward the oxidative pentose pathway of *Synechocystis* sp. PCC 6803 (Takeya et al., 2018). Accumulation of 2-hydroxy-3-methylvalerate could be due to the fermentation shift. Gammacurta et al. (2018) showed that branched

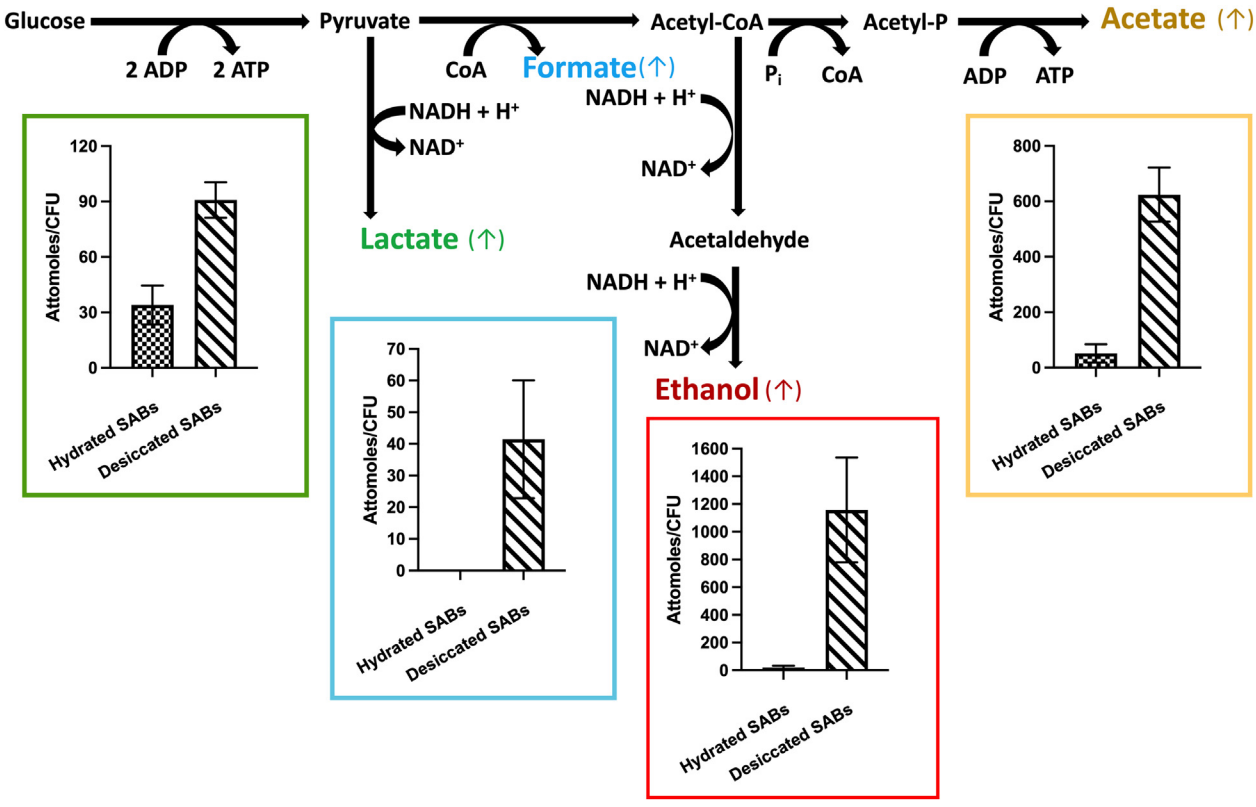

Fig. 3. Metabolite concentrations quantified via ^{1}H NMR spectra of hydrated and desiccated SABs indicate changes in the mixed-acid fermentation pathway. Identified metabolites within this pathway include lactate, formate, ethanol, and acetate; concentration changes are depicted above in each sample set.

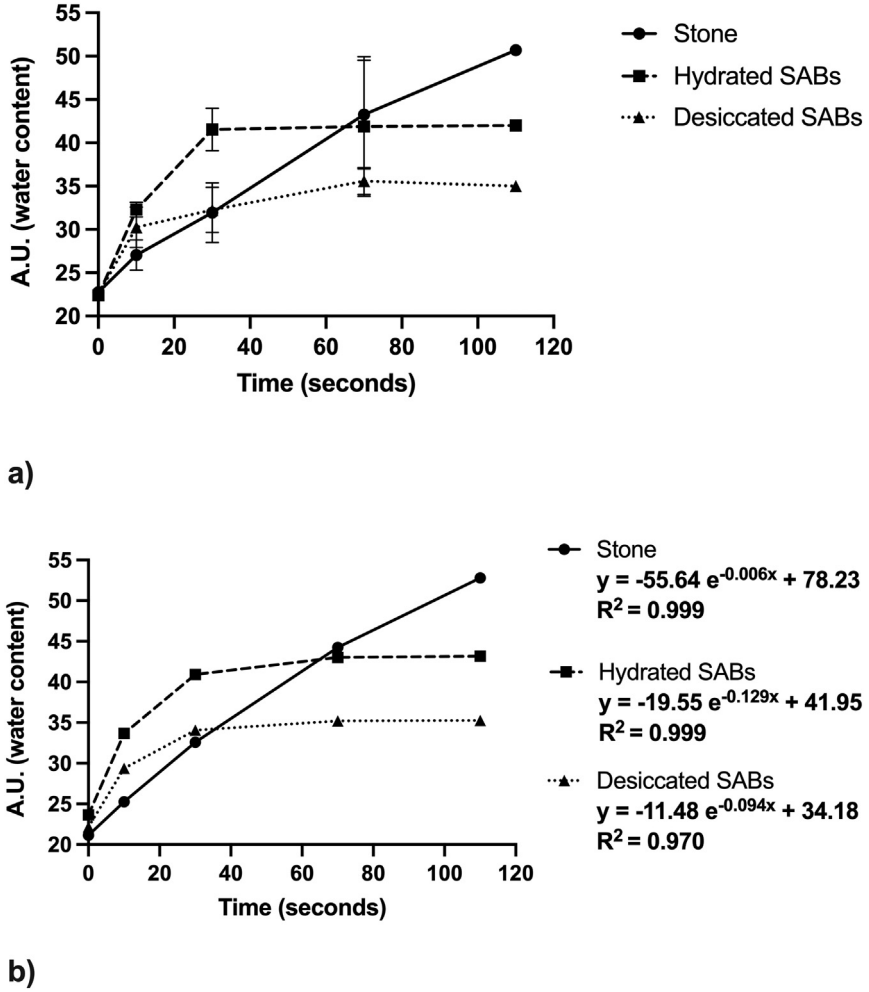

Fig. 4. Panel (a) Experimental data from MRI images. Water content in the stone pores in arbitrary units (A.U.) plotted against time in seconds. Panel (b) Regression model ($y = Ae^{-Bx} + C$) fitted to the mean of experimental data, the fitted equations, and the coefficients of determination (R^2). The asymptote of the curve, C, is the water saturation point.

hydroxylated esters, like ethyl 2-hydroxy-4-methylpentanoate, were the only compounds strongly influenced by the lactic acid bacteria fermentation in Bordeaux red wines. Basan et al. (2015) examined the metabolic savings of generating energy through aerobic respiration and the metabolic costs of synthesizing the enzymes and other biological apparatus required for fermentation and aerobic respiration within the bacterium *E. coli*. They concluded that, since the cost of protein synthesis overrules the metabolic savings for fast-growing cells, the cells under stress conditions preferred fermentation over respiration because it is more proteome efficient.

Desiccation caused the accumulation of amino acids (aspartate, alanine, arginine, and leucine) and nucleosides (cytidine, guanosine, uridine, adenosine) with 1.5- to 3.5-fold concentration increase. Protein and RNA syntheses are low in non-growing cells compared to growing cells, and accordingly, under stress, *E. coli* increases metabolites related to the degradation pathways for amino acids and nucleotides (Radoš et al., 2022). In the pyrimidine salvage pathway of *E. coli*, cytidine and uridine give rise to UTP (uridine-triphosphate) and CTP (cytidine-triphosphate)—substrates for the synthesis of RNA (Andersen et al., 1995). Thus, we speculated that RNA degradation led to the accumulation of adenosine and guanosine, but this degradation could have occurred in *Synechocystis* as well (Zhang et al., 2022). Interestingly, mRNA degradation regulates the activity of the central carbon metabolism and metabolic responses to stress (Roux et al., 2022). As arginine and leucine have the potential to control almost all amino acid biosynthesis pathways (Radoš et al., 2022), we hypothesized that their abundance is related to the capacity of cells to begin growing as promptly as the environmental conditions return favorably.

In our experiments, the accumulation of trehalose and betaine decreased in the desiccated SABs. Trehalose and glycine betaine were proposed as stress effectors against desiccation (osmolytes) because they were found in nearly all anhydrobiotes and they could mitigate desiccation-induced damage in many microorganisms (Klähn and Hagemann, 2011; Zhang and Yan, 2012). Our findings are in contrast with other works that reported an increase in the osmolytes concentration under desiccation (Sakamoto et al., 2009; Tapia and Koshland, 2014).

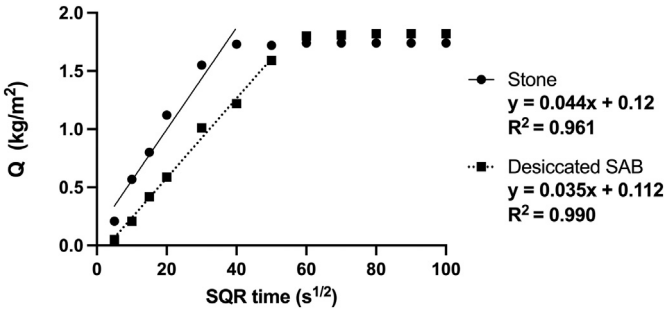

Fig. 5. A_{cap} values for stone specimens without and with desiccated SAB. The linear interpolations of data over the square root of time are done for the first 20 min (about 35 $s^{1/2}$) as suggested by the UNI EN standard. The data refer to a single experiment considered representative of the phenomenon observed. Replicates are reported in Supplementary materials (Supplementary materials S2).

The osmolytes trehalose and betaine are also synthesized in presence of a saline stress (Singh et al., 2022). The presence of trehalose and betaine in hydrated SAB is not surprising as mineral substrates such as limestone release water-soluble salts on the surface (Lamar and Shorde, 1953), and the SAB-dwelling cells are well acclimated to the salinity (Villa and Cappitelli, 2019). Thus, the osmolytes that protect SABs against salt stress and desiccation can also act as potent carbohydrate storage providing a nutrient source under unfavorable conditions. The impairment of trehalose synthesis results in a higher glucose availability (Laskowska and Kuczyńska-Wiśnik, 2020), which can be used for respiration or fermentation. *E. coli* contains periplasmic and cytoplasmic trehalases that catalyze the hydrolysis of trehalose into two molecules of D-glucose.

3.2. Desiccated SABs affect the water transport properties of the stone pores

Nuclear Magnetic Resonance Imaging (MRI) provides a tool to visualize the presence of water inside the stone pores and, hence, the effects of hydrated and desiccated SABs on water penetration in geomaterials. In our experiments, SABs colonized only the upper side of the specimens, and MRI was applied to evaluate water absorption from the bottom of the stone specimen toward its core. Fig. 4 displays the water content in the stone over time (Images available in Supplementary materials S1). Water absorption for hydrated and desiccated SABs was very rapid for the first 10 s and then eventually reached saturation point after 30 s (Fig. 4a). Since the solution to a simple diffusion problem is complementary to the inverse exponential form, this form is fitted to calculate the maximum theoretical water content (saturation point) for each condition as shown in Fig. 4b. The calculated saturation points for the stones with hydrated and desiccated SABs were 41.95 and 34.18 A.U., respectively. Meanwhile, the SAB-free stones (control samples) continued to absorb water over time until a calculated saturation point of 78.23 A.U. Overall, the water content in the stone in descending order is the following: SAB-free stone > hydrated SABs > desiccated SABs.

In order to corroborate the MRI results, the capillary water absorption coefficients (A_{cap}) were determined for both the control and desiccated SAB samples. The MRI was based on the diffusion from the bottom of the stone, while the A_{cap} was from the top of the stone, meaning from the part covered by the SAB.

Fig. 5 shows the means of cumulative water inflow per unit area (kg/m^2) plotted against the square root of time ($s^{1/2}$) during the first 3 h. The angular coefficients of the linear trend of the curves—the A_{cap} values—signified the water absorption rate of the colonized and uncolonized stone surfaces. The capillary water absorption performance of the stones with desiccated SABs (0.035 $kg/(m^2\ s^{1/2}) \pm 0.01$) was statistically significantly lower (*t*-test $p \leq 0.05$) than that of the control samples (0.044 $kg/(m^2\ s^{1/2}) \pm 0.02$), suggesting that the biofilms had modified the water absorption characteristic of the stone. Despite the fact that MRI and A_{cap} experiments investigated water diffusion inside the stone from different perspectives (downwards vs. upwards suction) and at different time scales (seconds vs. hours), both methods found that the water absorbance for the control samples was higher than the colonized samples over time.

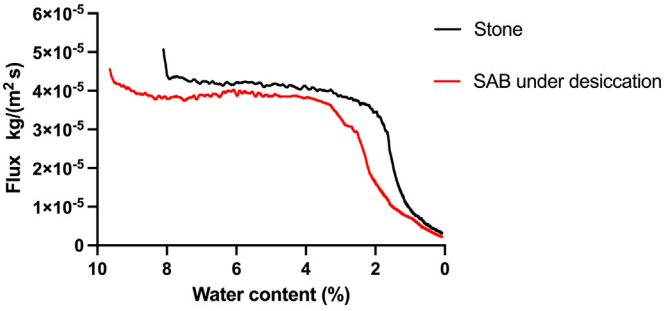

Fig. 7. Evaporation flux of the limestone specimen without (black line) and with dual-species SABs (red line). The plateaus on the curves (between 8 % and 4 % of water content) are considered the mean values of evaporation flux. The data refer to a single experiment considered representative of the phenomenon observed. Replicates are reported in Supplementary materials (Supplementary materials S3).

We also investigated the impact of SABs on water evaporation using thermography, which is based on the cooling process of water during the liquid-gas phase transition. Moistened samples without and with SABs were naturally air-dried at 25 °C and 50 % relative humidity. The evaporation was monitored for 5 h, the amount of time when the stone with SABs equilibrated with the ambient condition.

Fig. 6 shows the thermal images at different times during the drying process. The image at T0 displays the fully moistened samples (saturation condition) and the evaporation that cools the surface of both samples homogenously (deep blue). The surface temperature homogeneity suggested that fully hydrated SABs do not affect evaporative cooling despite being sparsely distributed. This finding could be explained by capillary transport: water is rapidly redistributed throughout the stone porous network while the water content remains uniform at the stone surface.

Thus, in moist condition (saturation of the pores), the presence of SABs neither repel water nor accelerate evaporation, suggesting that SABs do not completely clog the pores. Notably, when the water had evaporated at 254 and 280 min, meaning the evaporation had ceased, the sample temperature began to rise, indicating a dried surface (light blue). This phenomenon was very evident in the control samples, which lead to the conclusion that desiccated SABs retard evaporation from the lithic substrate. It seems that a SAB acts as a sponge and retains moisture only under critical conditions such as water stress. The SAB's spongy behavior was evident as shown at T280, while the colonized side of the stone was still cold and evaporating (left side), the rest of the side without the biofilm (right side) had started to warm up as an indication of a dry condition.

This important result was corroborated by the evaporation flux measurements using an analytical balance as shown in Fig. 7. The large plateau in the curves indicated a constant evaporation flux that corresponded to the phase where capillary action to the surface was more rapid than the evaporation at the surface (that is a gas diffusion process) (Ludwig et al., 2018; Melada et al., 2020a,b). The significantly different fluxes (*t*-test, $p \leq$

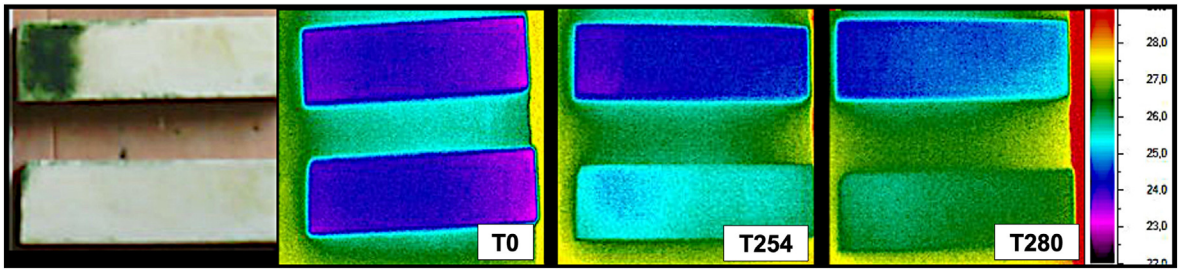

Fig. 6. Representative thermography images of the evaporation of wet stone in ambient conditions. The top and bottom stones are the dual-species SAB and the control sample under desiccation; respectively. a) visible image; b) evaporation at the saturation condition, T0; c) after 254 min, T254; d) after 280 min, T280.

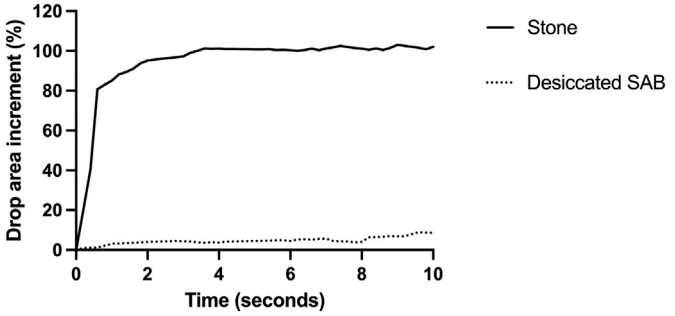

Fig. 8. Results from the spilling drop test. The solid and dotted lines represent the evolution of the drop in surfaces without (stone) and with desiccated SABs, respectively. The data refer to a single experiment considered representative of the phenomenon observed. Replicates are reported in Supplementary materials (Supplementary materials S5).

0.05) between the control and the colonized sample—$4.01 \pm 0.06 \times 10^{-5}$ kg/(m^2 s) and $3.78 \pm 0.08 \times 10^{-5}$ kg/(m^2 s) $\pm 0.08 \times 10^{-5}$, respectively—indicated that the desiccated SABs reduced the evaporation process. This could be attributed to the reduction in the size of superficial pores, exactly where the water exchange between the stone and the air takes place.

The effect of desiccated SABs on the wetting properties of the stone surface—as SABs were suspected to alter absorption and evaporation—was investigated using the spilling drop test. In fact, this test measured the stone's diffusion characteristic of liquid water at the surface. The areas with desiccated SABs were precisely identified by UV fluorescence prior to being used for the spilling drop tests (Supplementary materials S4).

Fig. 8 shows the increasing area of the water drop on the limestone with and without desiccated SABs, where there was a clear difference between the colonized and uncolonized areas. In the SAB-free area, the water spread in the limestone and doubled (+100 %) the initial drop area after 4 s. The presence of desiccated SAB was proven to dramatically reduce the water spread over the limestone surface. Considering previous observations on evaporation rate, we could not conclude that the presence of the desiccated SAB had transformed the stone into a water-repellent surface. Rather, the SAB had retarded the penetration of water into the pores, most likely binding the water with a mechanism that is faster and more efficient than capillary transport.

Microbial growth on stones can play an important role in deterioration, yet it can also favor protection. Water is known to promote stone weathering, hence, anything that interferes with water content could have long-term negative or positive repercussions on the stability of the built heritage. In agreement with our results, Coombes and Naylor (2012) observed reduced water absorption and evaporation on field-exposed crusted concrete, while Concha-Lozano et al. (2012) highlighted a hydraulic conductivity drop of the geomaterial in the presence of biofilm matrix. Cutler et al. (2013) showed that in the immediate subsurface, the areas with SABs had higher resistivity (meaning lower moisture content) than the ones without. Slavík et al. (2017) demonstrated that the sandstone with biologically-initiated rock crust had a slower water absorption rate compared to that without the crust. Recently, Schröer et al. (2022) reported that stones colonized by a cyanobacterial SAB experienced a slight reduction in both the capillary coefficient and the drying rate compared to the uncolonized stones. These effects can be related to the features of the SAB, such as the biofilm thickness and the composition of the EPM, as well as the structural and functional profile of the microbial community.

Overall, our findings indicated that desiccated SABs had counteracted the moisture variation inside the stone by reducing the water input and delaying the water output. McCabe et al. (2015) suggested that biofilms trap the moisture inside the stone, making it non-breathable, accumulating water at each wetting cycle, and ultimately increasing the risk of weathering. However, in presence of desiccated SABs, we observed in our experiments a reduction in capillary water absorption rate and in water saturation point. These results, combined with the 'hydrophobization' of the surface as displayed by the spilling drop test, suggested that desiccated SABs delay water absorption. In addition, the constant level of moisture in the stone might prevent water-induced deterioration phenomena such as salt weathering, freeze-thaw, and dry-wet cycles. Grondona et al. (1997) found that under the biofilm, the humidity was maintained at a constant level, therefore, avoiding sandstone surface weathering of uncovered areas. In fact, the SAB-covered sandstone did not experience salt crystal formation within the pores. Grondona et al. (1997) speculated that the overall stability of water content, due to the decrease in the capillary water absorption rate and the reduced water release by SABs, can have a protective effect in the field.

3.3. Relative humidity affects SAB rehydration and stone swelling

Periods of desiccation and rewetting are regular, yet stressful events encountered by SABs on stone monuments. To examine the effects of SAB's recovery after rewetting, desiccated SABs were exposed to increasing levels of relative humidity from 25 % to 90 %. During rewetting experiments, the live cell imaging showed that the recovery of both GFP (*E. coli*) and red chlorophyll fluorescence (*Synechocystis*) occurred simultaneously as soon as the relative humidity reached 70 % (Fig. 9a). The red autofluorescence of *Synechocystis* was due to the photosynthetic pigment and was considered an indicator of cell viability because related to the integrity of the photosynthetic apparatus (Roldán et al., 2014). GFP provides a sensitive, noninvasive marker for cell viability in both bacteria and fungi (Lehtinen et al., 2004; Nichols et al., 2018). Thus, the desiccated SABs recover their activities quickly after reaching a critical relative humidity. SABs respond quickly and efficiently to hydration by exploiting this short window of opportunity to secure the nutrients (Baubin et al., 2022). The water was possibly formed, at least partially, by the deliquescence of salts, a process when hygroscopic salts absorb ambient water vapor and form a saturated brine. The presence of salts in building materials can originate internally or externally, for example, the original geomaterials, an uplift of salt water from the ocean, the decomposition of the mineral constituents, and the deposition of atmospheric pollutants through the rain (Li and Gu, 2022). Thus, if there were deliquescent salts in the stone pores, there would be a chance for the SABs to capture ambient water vapor. Davila et al. (2013) observed that the photosynthetic systems of cyanobacteria inside the halite crusts of the Atacama desert become active when the relative humidity rises above 70 % and the salt becomes wet for deliquescent. Li and Gu (2022) reported that when the relative humidity exceeds 70 %, liquid water with mobility is formed within the stone pores, promoting microbial colonization. Gaylarde and Little (2022) reported that atmospheric relative humidity above 70 % can be sufficient to sustain the photosynthetic activity of algae and cyanobacteria in rocks. Similarly, both the cyanobacterium and the heterotroph of the desiccated SAB recovered activity with a relative humidity of 70 %, similar to the deliquescence-based photosynthesis in the aforementioned desert ecosystems.

The video obtained from CLSM (Supplementary material S6) shows that the stone underneath the SAB was swelling with increasing relative humidity. Using image analysis software, we found that the vertical swelling occurred at RH above 70 %, while in the presence of desiccated SAB, the swelling was reduced to 52.8 % (Fig. 9b). Thus, the presence of a desiccated SAB reduces the hygric expansion of limestone specimens in humid conditions.

The moisture-driven expansion of a geomaterial is one of the most important factors in stone deterioration and this expansion is mostly associated with the swelling of clay minerals. Sedimentary stones, such as limestones, usually contain a portion of clay minerals in their matrix (Aly et al., 2020). The damage by swelling clays in stones has been recognized as a major problem in the conservation of cultural heritage (Elert and Rodriguez-Navarro, 2022). The main process of clay swelling is the so-called intracrystalline swelling, which is the incorporation of successive water monolayers in the interlayer space of the swelling clays (Chen et al., 2022). The water produced by salt deliquescence in the stone pores can swell the clays that can irreversibly damage the internal structure of the stone by forming and propagating cracks. The deliquescence-induced liquid water is immediately sequestered by the desiccated SAB and is

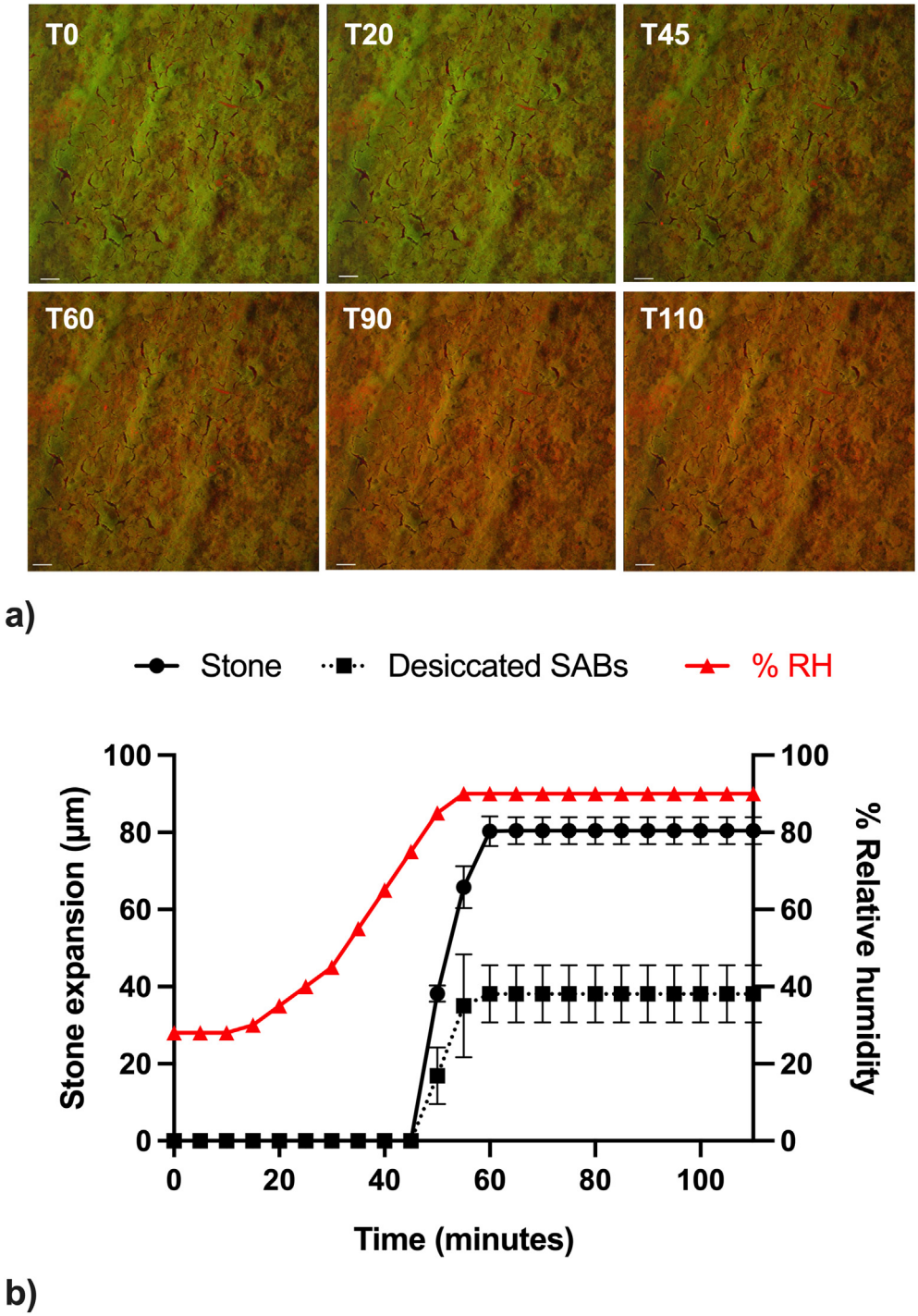

Fig. 9. In panel (a) 3D CLSM images of the dual-species SAB during the rewetting experiment. The pictures display the recovery of fluorescence of a dual-species SAB during rewetting. The bars in the CLSM images represent 150 µm. The graph in panel (a) reports the stone expansion after rewetting in the absence and in presence of a desiccated SAB.

then unavailable for the swollen clay minerals. In this way, the SAB would have liquid water for photosynthesis and would simultaneously reduce stone expansion. After all, the EPM is a hydrogel that will absorb water until the equilibrium swelling is reached (Seminara et al., 2012).

4. Conclusion

The SABs' response to drought varies depending on the microbiome's physiological tolerance and metabolic flexibility. In the dual-species SAB, the metabolism shifted to fermentation that produces ethanol and organic acids (e.g., acetic, lactic, and formic acids), which might facilitate mineral dissolution and stone degradation. However, we do not know if the organic acids produced can actually reach the stone surface and dissolve the material. The organic acids could possibly be consumed by other components in the SAB community and transformed into harmless compounds by microbial metabolisms. The diffusion of organic acids through the SAB might also be reduced by the absence of free water and the increased viscosity of the eDNA-enriched EPM after the desiccation (Campoccia et al., 2021; Seviour et al., 2021). The acids could also be produced in minute quantities as reported by Schröer et al. (2020), where the isolates from the SABs taken

from the Lede stone in an urban environment did not produce a significant amount of acids in the laboratory.

It was clear that desiccated dual-species SABs affected the flux of water between the substrate and the environment, showing a moisture-controlling feature. The dual-species SABs keep a constant moisture content in the stone, reducing its hydraulic stresses. The measured rate of the water capillary action showed that the dual-species SABs protect the stone from rapid water absorption, while the thermographic survey documented a delay in water evaporation from the stone. Worth noting was the observation that the SABs' moisture-controlling effect is exerted on the whole stone specimen, despite the patchy distribution of the biofilms. Thus, we can assume that a continuous distribution of SABs over the lithic surface might further exacerbate the differences in water-related dynamics between uncolonized and colonized limestones. After all, Mottershead et al. (2003) reported a reduction in the sandstone weathering rate where a homogeneous distribution of SABs was present. Moreover, the spilling-drop tests indicated a reduced wettability of the surface in presence of desiccated dual-species SABs, which affect both the water absorption and water diffusion rates inside the stone. This is possible by assuming a sort of sponge effect by the SABs that retain water in the biofilm-stone system superseding the capillary action in the same system. From a conservation perspective, it is important to emphasize that—below certain thresholds of water saturation—it is not the water content that damages the stone, but rather the dry-wet cycle (Menéndez, 2018). The frequency and amplitude of this dry-wet cycle control the efficacy of the decaying processes, which can be particularly destructive to building stones that contain swelling-prone clays (Sass and Viles, 2022).

It is generally agreed that climate change is affecting stone decay, and historic buildings are likely to become increasingly vulnerable to moisture-induced deterioration. For example, intense precipitation and flooding after a long period of drought might deepen the wetting front and change the saturation threshold of the geomaterial, increasing frost and salt weathering. However, to gain a more complete picture of the relationship between climate change and heritage decay, it is necessary to understand the hydrology of stone-SAB ecosystems. Currently, scientists have limited knowledge of moisture dynamics at the biofilm and stone levels. The moisture spatio-temporal patterns and saturation threshold of the stones with and without SABs are still unclear. For instance, since the biofilm EPM is a hydrogel that can absorb and store water extensively, it may affect the moisture dynamics of the geomaterial. Thus, a conceptual framework of heritage hydrology that considers both mineral and biological components is needed for a holistic understanding of moisture-induced deterioration, which will ultimately improve the sustainable management of cultural heritage under climate change.

Overall, these findings suggested that a desiccated dual-species SAB underwent substantial structural and metabolic reprogramming that modified the stone surface. This interfacial modification of the stone acted as a buffering layer that preserved the lithic material from moisture fluctuations. We are aware that SABs in natural settings may have different compositions that affect biofilm behavior and, consequently, different impacts on stone substrates. The majority of the scientific literature is still underestimating or neglecting the bioprotective role of biofilms on artistic surfaces. This work has provided evidence that SABs can have a bioprotective effect on water-induced and water-related deterioration. Thus, the choice of removing a SAB or keeping it in place should be carefully evaluated case by case.

Supplementary data to this article can be found online at https://doi.org/10.1016/j.scitotenv.2023.161666.

CRediT authorship contribution statement

F. Villa: Conceptualization, Investigation, Formal analysis, Visualization, Data curation, Writing – original draft, Writing – review & editing. **N. Ludwig:** Conceptualization, Investigation, Formal analysis, Visualization, Data curation, Writing – original draft, Writing – review & editing. **S. Mazzini:** Methodology, Investigation, Formal analysis, Writing – review & editing. **L. Scaglioni:** Methodology, Investigation, Formal analysis, Writing – review & editing. **A.L. Fuchs:** Methodology, Investigation, Formal analysis, Writing – review & editing. **B. Tripet:** Methodology, Investigation, Formal analysis, Writing – review & editing. **V. Copié:** Methodology, Investigation, Formal analysis, Visualization, Writing – review & editing, Resources. **P.S. Stewart:** Methodology, Writing – review & editing, Resources, Supervision. **F. Cappitelli:** Conceptualization, Writing – review & editing, Resources, Supervision.

Data availability

Data will be made available on request.

Declaration of competing interest

The authors declare that they have no known competing financial interests or personal relationships that could have appeared to influence the work reported in this paper.

Acknowledgments

^{1}H NMR spectra were recorded at Montana State University on a Bruker 600 MHz (1H Larmor frequency) solution NMR spectrometer housed in MSU's NMR Core Facility. Financial support for the NMR instruments and operations of the Facility has been provided in part by the NIH SIG program (1S10RR13878 and 1S10RR026659), the National Science Foundation (NSF-MRI:DBI-1532078), the Murdock Charitable Trust Foundation (2015066:MNL), and MSU's office of the Vice President for Research. The authors thank Mr. Pancasatya Agastra Kusnandar for the English editing.

References

Acuña, V., Casellas, M., Corcoll, N., Timoner, X., Sabater, S., 2015. Increasing extent of periods of no flow in intermittent waterways promotes heterotrophy. Freshw. Biol. 60, 1810–1823. https://doi.org/10.1111/fwb.12612.

Albertano, P., 2012. Cyanobacterial biofilms in monuments and caves. In: Whitton, B.A. (Ed.), Ecology of Cyanobacteria II: Their Diversity in Space and Time. Springer, Netherlands, Dordrecht, pp. 317–343 https://doi.org/10.1007/978-94-007-3855-3_11.

Aly, N., Hamed, A., El-Al, A.A., 2020. The impact of hydric swelling on the mechanical behavior of Egyptian helwan limestone. Period.Polytech.Civ.Eng. 64, 589–596. https://doi.org/10.3311/PPci.15360.

Andersen, P.S., Frees, D., Fast, R., Mygind, B., 1995. Uracil uptake in Escherichia coli K-12: isolation of uraA mutants and cloning of the gene. J. Bacteriol. 177, 2008–2013. https://doi.org/10.1128/jb.177.8.2008-2013.1995.

Angermayr, S.A., van Alphen, P., Hasdemir, D., Kramer, G., Iqbal, M., van Grondelle, W., Hoefsloot, H.C., Choi, Y.H., Hellingwerf, K.J., 2016. Culturing synechocystis sp. strain PCC 6803 with N2 and CO2 in a diel regime reveals multiphase glycogen dynamics with low maintenance costs. Appl. Environ. Microbiol. 82, 4180–4189. https://doi.org/10.1128/AEM.00256-16.

Bar-Eyal, L., Eisenberg, I., Faust, A., Raanan, H., Nevo, R., Rappaport, F., Krieger-Liszkay, A., Sétif, P., Thurotte, A., Reich, Z., Kaplan, A., Ohad, I., Paltiel, Y., Keren, N., 2015. An easily reversible structural change underlies mechanisms enabling desert crust cyanobacteria to survive desiccation. Biochim. Biophys. Acta Bioenerg. 1847, 1267–1273. https://doi.org/10.1016/j.bbabio.2015.07.008.

Bartoli, F., Municchia, A.C., Futagami, Y., Kashiwadani, H., Moon, K.H., Caneva, G., 2014. Biological colonization patterns on the ruins of Angkor temples (Cambodia) in the biodeterioration vs bioprotection debate. Int. Biodeterior. Biodegradation 96, 157–165. https://doi.org/10.1016/j.ibiod.2014.09.015.

Basan, M., Hui, S., Okano, H., Zhang, Z., Shen, Y., Williamson, J.R., Hwa, T., 2015. Overflow metabolism in Escherichia coli results from efficient proteome allocation. Nature 528, 99–104. https://doi.org/10.1038/nature15765.

Bastian, F., Jurado, V., Nováková, A., Alabouvette, C., Saiz-Jimenez, C.Y., 2010. n.d. The microbiology of Lascaux Cave. Microbiology 156, 644–652. https://doi.org/10.1099/mic.0.036160-0.

Baubin, C., Ran, N., Siebner, H., Gillor, O., 2022. Divergence of biocrust active bacterial communities in the Negev Desert during a hydration-desiccation cycle. Microb. Ecol. https://doi.org/10.1007/s00248-022-02063-z.

Bellinzoni, A.M., Caneva, G., Ricci, S., 2003. Ecological trends in travertine colonisation by pioneer algae and plant communities. Int. Biodeterior. Biodegradation 51, 203–210. https://doi.org/10.1016/S0964-8305(02)00172-5.

Branysova, T., Demnerova, K., Durovic, M., Stiborova, H., 2022. Microbial biodeterioration of cultural heritage and identification of the active agents over the last two decades. J. Cult. Herit. 55, 245–260. https://doi.org/10.1016/j.culher.2022.03.013.

Campoccia, D., Montanaro, L., Arciola, C.R., 2021. Extracellular DNA (eDNA). A major ubiquitous element of the bacterial biofilm architecture. Int. J. Mol. Sci. 22, 9100. https://doi.org/10.3390/ijms22169100.

Carter, N.E.A., Viles, H.A., 2005. Bioprotection explored: the story of a little known earth surface process. Geomorphology 67, 273–281. https://doi.org/10.1016/j.geomorph.2004.10.004.

Chen, W.L., Grabowski, R.C., Goel, S., 2022. Clay swelling: role of cations in stabilizing/destabilizing mechanisms. ACS Omega 7, 3185–3191. https://doi.org/10.1021/acsomega.1c04384.

Chong, J., Soufan, O., Li, C., Caraus, I., Li, S., Bourque, G., Wishart, D.S., Xia, J., 2018. MetaboAnalyst 4.0: towards more transparent and integrative metabolomics analysis. Nucleic Acids Res. 46, W486–W494. https://doi.org/10.1093/nar/gky310.

Concha-Lozano, N., Gaudon, P., Pages, J., de Billerbeck, G., Lafon, D., Eterradossi, O., 2012. Protective effect of endolithic fungal hyphae on oolitic limestone buildings. J. Cult. Herit. 13, 120–127. https://doi.org/10.1016/j.culher.2011.07.006.

Coombes, M.A., Naylor, L.A., 2012. Rock warming and drying under simulated intertidal conditions, part II: weathering and biological influences on evaporative cooling and near-surface micro-climatic conditions as an example of biogeomorphic ecosystem engineering. Earth Surf. Process. Landf. 37, 100–118. https://doi.org/10.1002/esp.2232.

Crausbay, S.D., Ramirez, A.R., Carter, S.L., Cross, M.S., Hall, K.R., Bathke, D.J., Betancourt, J.L., Colt, S., Cravens, A.E., Dalton, M.S., Dunham, J.B., Hay, L.E., Hayes, M.J., McEvoy, J., McNutt, C.A., Moritz, M.A., Nislow, K.H., Raheem, N., Sanford, T., 2017. Defining ecological drought for the twenty-first century. Bull. Am. Meteorol. Soc. 98, 2543–2550.

Cutler, N.A., Viles, H.A., Ahmad, S., McCabe, S., Smith, B.J., 2013. Algal 'greening' and the conservation of stone heritage structures. Sci. Total Environ. 442, 152–164. https://doi.org/10.1016/j.scitotenv.2012.10.050.

Davila, A.F., Hawes, I., Ascaso, C., Wierzchos, J., 2013. Salt deliquescence drives photosynthesis in the hyperarid Atacama Desert. Environ. Microbiol. Rep. 5, 583–587. https://doi.org/10.1111/1758-2229.12050.

Davis, M.C., Messina, M.A., Nicolosi, G., Petralia, S., Iv, M.D.B., Mayne, C.K.S., Dinon, C.M., Moss, C.J., Onac, B.P., Garey, J.R., 2020. Surface runoff alters cave microbial community structure and function. PLOS ONE 15, e0232742. https://doi.org/10.1371/journal.pone.0232742.

Elert, K., Rodriguez-Navarro, C., 2022. Degradation and conservation of clay-containing stone: a review. Constr. Build. Mater. 330, 127226. https://doi.org/10.1016/j.conbuildmat.2022.127226.

Elias, S., Banin, E., 2012. Multi-species biofilms: living with friendly neighbors. FEMS Microbiol. Rev. 36, 990–1004. https://doi.org/10.1111/j.1574-6976.2012.00325.x.

Favero-Longo, S.E., Viles, H.A., 2020. A review of the nature, role and control of lithobionts on stone cultural heritage: weighing-up and managing biodeterioration and bioprotection. World J. Microbiol. Biotechnol. 36, 100. https://doi.org/10.1007/s11274-020-02878-3.

Fernandez-Cortes, A., Cuezva, S., Sanchez-Moral, S., Cañaveras, J.C., Porca, E., Jurado, V., Martin-Sanchez, P.M., Saiz-Jimenez, C., 2011. Detection of human-induced environmental disturbances in a show cave. Environ. Sci. Pollut. Res. 18, 1037–1045. https://doi.org/10.1007/s11356-011-0513-5.

Fuchs, A., Tripet, B.P., Ammons, M.C.B., Copié, V., 2016. Optimization of metabolite extraction protocols for the identification and profiling of small molecule metabolites from planktonic and biofilm Pseudomonas aeruginosa cultures. Curr. Metabolomics 4, 141–147. https://doi.org/10.2174/2213235x04666151126203043.

Fuchs, A.L., Schiller, S.M., Keegan, W.J., Ammons, M.C.B., Eilers, B., Tripet, B., Copié, V., 2019. Quantitative 1H NMR metabolomics reveal distinct metabolic adaptations in human macrophages following differential activation. Metabolites 9, 248. https://doi.org/10.3390/metabo9110248.

Fuentes, E., Vázquez-Nion, D., Prieto, B., 2022. Laboratory development of subaerial biofilms commonly found on buildings.A methodological review. Build. Environ. 223, 109451. https://doi.org/10.1016/j.buildenv.2022.109451.

Gammacurta, M., Lytra, G., Marchal, A., Marchand, S., Christophe Barbe, J., Moine, V., de Revel, G., 2018. Influence of lactic acid bacteria strains on ester concentrations in red wines: specific impact on branched hydroxylated compounds. Food Chem. 239, 252–259. https://doi.org/10.1016/j.foodchem.2017.06.123.

García-Fontana, C., Narváez-Reinaldo, J.J., Castillo, F., González-López, J., Luque, I., Manzanera, M., 2016. A new physiological role for the DNA molecule as a protector against drying stress in desiccation-tolerant microorganisms. Front. Microbiol. 7, 2066. https://doi.org/10.3389/fmicb.2016.02066.

Gaylarde, Peter, Gaylarde, Christine, 2004. Deterioration of siliceous stone monuments in Latin America: microorganisms and mechanisms. Corros. Rev. 22, 395–416. https://doi.org/10.1515/CORRREV.2004.22.5-6.395.

Gaylarde, C., Little, B., 2022. Biodeterioration of stone and metal — fundamental microbial cycling processes with spatial and temporal scale differences. Sci. Total Environ. 823, 153193. https://doi.org/10.1016/j.scitotenv.2022.153193.

Gaylarde, C.C., Rodríguez, C.H., Navarro-Noya, Y.E., Ortega-Morales, B.O., 2012. Microbial biofilms on the sandstone monuments of the Angkor Wat Complex, Cambodia. Curr. Microbiol. 64, 85–92. https://doi.org/10.1007/s00284-011-0034-y.

Gaylarde, C., Baptista-Neto, J.A., Ogawa, A., Kowalski, M., Celikkol-Aydin, S., Beech, I., 2017. Epilithic and endolithic microorganisms and deterioration on stone church facades subject to urban pollution in a sub-tropical climate. Biofouling 33, 113–127. https://doi.org/10.1080/08927014.2016.1269893.

Goller, C.C., Romeo, T., 2008. Environmental influences on biofilm development. Curr. Top. Microbiol. Immunol. 322, 37–66. https://doi.org/10.1007/978-3-540-75418-3_3.

Gorbushina, A.A., 2007. Life on the rocks. Environ. Microbiol. 9, 1613–1631. https://doi.org/10.1111/j.1462-2920.2007.01301.x.

Grondona, I., Monte, E., Rives, V., Vicente, M.A., 1997. Lichenized association between Septonema tormes sp. nov., a coccoid cyanobacterium, and a green alga with an unforeseen biopreservation effect of Villamayor sandstone at 'Casa Lis' of Salamanca,Spain. Mycol. Res. 101, 1489–1495. https://doi.org/10.1017/S0953756297004309.

Grzyb, T., Skłodowska, A., 2022. Introduction to bacterial anhydrobiosis: a general perspective and the mechanisms of desiccation-associated damage. Microorganisms 10, 432. https://doi.org/10.3390/microorganisms10020432.

Gulotta, D., Villa, F., Cappitelli, F., Toniolo, L., 2018. Biofilm colonization of metamorphic lithotypes of a renaissance cathedral exposed to urban atmosphere. Sci. Total Environ. 639, 1480–1490. https://doi.org/10.1016/j.scitotenv.2018.05.277.

Hu, W., Li, L., Sharma, S., Wang, J., McHardy, I., Lux, R., Yang, Z., He, X., Gimzewski, J.K., Li, Y., Shi, W., 2012. DNA builds and strengthens the extracellular matrix in Myxococcus xanthus biofilms by interacting with exopolysaccharides. PLOS ONE 7, e51905. https://doi.org/10.1371/journal.pone.0051905.

Ibáñez de Aldecoa, A.L., Zafra, O., González-Pastor, J.E., 2017. Mechanisms and regulation of extracellular DNA release and its biological roles in microbial communities. Front. Microbiol. 8, 1390. https://doi.org/10.3389/fmicb.2017.01390.

Ikner, L.A., Toomey, R.S., Nolan, G., Neilson, J.W., Pryor, B.M., Maier, R.M., 2007. Culturable microbial diversity and the impact of tourism in Kartchner Caverns, Arizona. Microb. Ecol. 53, 30–42. https://doi.org/10.1007/s00248-006-9135-8.

Jakubowski, W., Biliński, T., Bartosz, G., 2000. Oxidative stress during aging of stationary cultures of the yeast Saccharomyces cerevisiae. Free Radic. Biol. Med. 28, 659–664. https://doi.org/10.1016/s0891-5849(99)00266-x.

Klähn, S., Hagemann, M., 2011. Compatible solute biosynthesis in cyanobacteria. Environ. Microbiol. 13, 551–562. https://doi.org/10.1111/j.1462-2920.2010.02366.x.

Kranner, I., Beckett, R., Hochman, A., Nash, T.H., 2008. Desiccation-tolerance in lichens: a review. Bryologist 111, 576–593.

Lamar, J.E., Shorde, R.S., 1953. Water soluble salts in limestone and dolomites. Econ. Geol. 48, 97–112. https://doi.org/10.2113/gsecongeo.48.2.97.

Laskowska, E., Kuczyńska-Wiśnik, D., 2020. New insight into the mechanisms protecting bacteria during desiccation. Curr. Genet. 66, 313–318. https://doi.org/10.1007/s00294-019-01036-z.

Lehtinen, J., Nuutila, J., Lilius, E.-M., 2004. Green fluorescent protein-propidium iodide (GFP-PI) based assay for flow cytometric measurement of bacterial viability. Cytometry A 60, 165–172. https://doi.org/10.1002/cyto.a.20026.

Leprince, O., Hoekstra, F.A., Harren, F.J.M., 2000. Unravelling the responses of metabolism to dehydration points to a role for cytoplasmic viscosity in desiccation tolerance. Seed biology: advances and applications. Proceedings of the Sixth International Workshop on Seeds, Merida, Mexico, 1999. CABI Books, pp. 57–66 https://doi.org/10.1079/9780851994048.0057.

Li, Y.-H., Gu, J.-D., 2022. A more accurate definition of water characteristics in stone materials for an improved understanding and effective protection of cultural heritage from biodeterioration. Int. Biodeterior. Biodegradation 166, 105338. https://doi.org/10.1016/j.ibiod.2021.105338.

Lianou, A., Nychas, G.-J.E., Koutsoumanis, K.P., 2020. Strain variability in biofilm formation: a food safety and quality perspective. Food Res. Int. 137, 109424. https://doi.org/10.1016/j.foodres.2020.109424.

Liu, X., Koestler, R.J., Warscheid, T., Katayama, Y., Gu, J.-D., 2020. Microbial deterioration and sustainable conservation of stone monuments and buildings. Nat. Sustain. 3, 991–1004. https://doi.org/10.1038/s41893-020-00602-5.

Liu, X., Qian, Y., Wu, F., Wang, Y., Wang, W., Gu, J.-D., 2022. Biofilms on stone monuments: biodeterioration or bioprotection? Trends Microbiol. 30, 816–819. https://doi.org/10.1016/j.tim.2022.05.012.

Ludwig, N., Rosina, E., Sansonetti, A., 2018. Evaluation and monitoring of water diffusion into stone porous materials by means of innovative IR thermography techniques. Measurement 118, 348–353. https://doi.org/10.1016/j.measurement.2017.09.002.

McCabe, S., McAllister, D., Warke, P.A., Gomez-Heras, M., 2015. Building sandstone surface modification by biofilm and iron precipitation: emerging block-scale heterogeneity and system response. Earth Surf. Process. Landf. 40, 112–122. https://doi.org/10.1002/esp.3665.

Melada, Jacopo, Arosio, P., Gargano, M., Ludwig, N., 2020. Multi-instrumental Characterization of Porous Media: The Role of the Spilling Drop Test. https://doi.org/10.21611/qirt.2020.061.

Melada, J., Arosio, P., Gargano, M., Veronese, I., Gallo, S., Ludwig, N., 2020. Optical reflectance apparatus for moisture content determination in porous media. Microchem. J. 154, 104627. https://doi.org/10.1016/j.microc.2020.104627.

Menéndez, B., 2018. Estimators of the impact of climate change in salt weathering of cultural heritage. Geosciences 8, 401. https://doi.org/10.3390/geosciences8110401.

Mottershead, D., Gorbushina, A., Lucas, G., Wright, J., 2003. The influence of marine salts, aspect and microbes in the weathering of sandstone in two historic structures. Building and Environment, Building Stone Decay: Observations, Experiments and Modeling. 38, pp. 1193–1204. https://doi.org/10.1016/S0360-1323(03)00071-4.

Naylor, L.A., Viles, H.A., Carter, N.E.A., 2002. Biogeomorphology revisited: looking towards the future. Geomorphology 47, 3–14. https://doi.org/10.1016/S0169-555X(02)00137-X.

Nichols, N.N., Quarterman, J.C., Frazer, S.E., 2018. Use of green fluorescent protein to monitor fungal growth in biomass hydrolysate. Biol. Methods Protoc. 3, bpx012. https://doi.org/10.1093/biomethods/bpx012.

Ortega-Morales, O., Guezennec, J., Hernández-Duque, G., Gaylarde, C.C., Gaylarde, P.M., 2000. Phototrophic biofilms on ancient mayan buildings in Yucatan, Mexico. Curr. Microbiol. 40, 81–85. https://doi.org/10.1007/s002849910015.

Palud, A., Salem, K., Cavin, J.-F., Beney, L., Licandro, H., 2020. Identification and transcriptional profile of Lactobacillus paracasei genes involved in the response to desiccation and rehydration. Food Microbiol. 85, 103301. https://doi.org/10.1016/j.fm.2019.103301.

Petrou, K., Trimborn, S., Kühl, M., Ralph, P.J., 2014. Desiccation stress in two intertidal beachrock biofilms. Mar. Biol. https://doi.org/10.1007/s00227-014-2458-y.

Pietramellara, G., Ascher, J., Borgogni, F., Ceccherini, M.T., Guerri, G., Nannipieri, P., 2009. Extracellular DNA in soil and sediment: fate and ecological relevance. Biol. Fertil. Soils 45, 219–235. https://doi.org/10.1007/s00374-008-0345-8.

Pinna, D., 2014. Biofilms and lichens on stone monuments: do they damage or protect? Front. Microbiol. 5, 133. https://doi.org/10.3389/fmicb.2014.00133.

Potts, M., 1999. Mechanisms of desiccation tolerance in cyanobacteria. Eur. J. Phycol. 34, 319–328. https://doi.org/10.1080/09670269910001736382.

Potysz, A., Bartz, W., 2022. Bioweathering of minerals and dissolution assessment by experimental simulations—implications for sandstone rocks: a review. Constr. Build. Mater. 316, 125862. https://doi.org/10.1016/j.conbuildmat.2021.125862.

Raanan, H., Oren, N., Treves, H., Keren, N., Ohad, I., Berkowicz, S.M., Hagemann, M., Koch, M., Shotland, Y., Kaplan, A., 2016. Towards clarifying what distinguishes cyanobacteria able to resurrect after desiccation from those that cannot: the photosynthetic aspect. Biochim. Biophys. Acta Bioenerg. 1857, 715–722. https://doi.org/10.1016/j.bbabio.2016.02.007.

Radoš, D., Donati, S., Lempp, M., Rapp, J., Link, H., 2022. Homeostasis of the biosynthetic E. coli metabolome. iScience 25, 104503. https://doi.org/10.1016/j.isci.2022.104503.

Rippka, R., Deruelles, J., Waterbury, J.B., Herdman, M., Stanier, R.Y.Y., 1979. n.d. Generic assignments, strain histories and properties of pure cultures of cyanobacteria. Microbiology 111, 1–61. https://doi.org/10.1099/00221287-111-1-1.

Roldán, M., Ascaso, C., Wierzchos, J., 2014. Fluorescent fingerprints of endolithic phototrophic cyanobacteria living within halite rocks in the Atacama Desert. Appl. Environ. Microbiol. 80, 2998–3006. https://doi.org/10.1128/AEM.03428-13.

Rosina, E., Ludwig, N., della torre, S., D'Ascola, S., Sotgia, C., Cornale, P., 2008. Thermal and hygroscopic characteristics of restored plasters with different surface textures. Mater. Eval. 66, 1271–1278.

Roux, C., Etienne, T.A., Hajnsdorf, E., Ropers, D., Carpousis, A.J., Cocaign-Bousquet, M., Girbal, L., 2022. The essential role of mRNA degradation in understanding and engineering E. coli metabolism. Biotechnol. Adv. 54, 107805. https://doi.org/10.1016/j.biotechadv.2021.107805.

Sabater, S., Timoner, X., Borrego, C., Acuña, V., 2016. Stream biofilm responses to flow intermittency: from cells to ecosystems. Front. Environ. Sci. 4.

Sakamoto, T., Yoshida, T., Arima, H., Hatanaka, Y., Takani, Y., Tamaru, Y., 2009. Accumulation of trehalose in response to desiccation and salt stress in the terrestrial cyanobacterium Nostoc commune. Phycol. Res. 57, 66–73. https://doi.org/10.1111/j.1440-1835.2008.00522.x.

Sanmartín, P., Villa, F., Cappitelli, F., Balboa, S., Carballeira, R., 2020. Characterization of a biofilm and the pattern outlined by its growth on a granite-built cloister in the Monastery of San Martiño Pinario (Santiago de Compostela, NW Spain). Int. Biodeterior. Biodegradation 147, 104871. https://doi.org/10.1016/j.ibiod.2019.104871.

Sass, O., Viles, H., 2022. Heritage hydrology: a conceptual framework for understanding water fluxes and storage in built and rock-hewn heritage. Herit.Sci. 10, 66. https://doi.org/10.1186/s40494-022-00693-7.

Schröer, L., De Kock, T., Cnudde, V., Boon, N., 2020. Differential colonization of microbial communities inhabiting lede stone in the urban and rural environment. Sci. Total Environ. 733, 139339. https://doi.org/10.1016/j.scitotenv.2020.139339.

Schröer, L., De Kock, T., Godts, S., Boon, N., Cnudde, V., 2022. The effects of cyanobacterial biofilms on water transport and retention of natural building stones. Earth Surf. Process. Landf. 47, 1921–1936. https://doi.org/10.1002/esp.5355.

Seminara, A., Angelini, T.E., Wilking, J.N., Vlamakis, H., Ebrahim, S., Kolter, R., Weitz, D.A., Brenner, M.P., 2012. Osmotic spreading of Bacillus subtilis biofilms driven by an extracellular matrix. Proc. Natl. Acad. Sci. 109, 1116–1121. https://doi.org/10.1073/pnas.1109261108.

Seviour, T., Winnerdy, F.R., Wong, L.L., Shi, X., Mugunthan, S., Foo, Y.H., Castaing, R., Adav, S.S., Subramoni, S., Kohli, G.S., Shewan, H.M., Stokes, J.R., Rice, S.A., Phan, A.T., Kjelleberg, S., 2021. The biofilm matrix scaffold of Pseudomonas aeruginosa contains G-quadruplex extracellular DNA structures. npj Biofilms Microbiomes 7, 1–12. https://doi.org/10.1038/s41522-021-00197-5.

Singh, R.P., Yadav, P., Kujur, R., Pandey, K.D., Gupta, R.K., 2022. Chapter10 - cyanobacteria and salinity stress tolerance. In: Singh, P., Fillat, M., Kumar, A. (Eds.), Cyanobacterial Lifestyle and Its Applications in Biotechnology. Academic Press, pp. 253–280 https://doi.org/10.1016/B978-0-323-90634-0.00003-2.

Slavík, M., Bruthans, J., Filippi, M., Schweigstillová, J., Falteisek, L., Řihošek, J., 2017. Biologically-initiated rock crust on sandstone: mechanical and hydraulic properties and resistance to erosion. Geomorphology 278, 298–313. https://doi.org/10.1016/j.geomorph.2016.09.040.

Stal, L.J., Moezelaar, R., 1997. Fermentation in cyanobacteria1. FEMS Microbiol. Rev. 21, 179–211. https://doi.org/10.1111/j.1574-6976.1997.tb00350.x.

Takeya, M., Iijima, H., Sukigara, H., Osanai, T., 2018. Cluster-level relationships of genes involved in carbon metabolism in Synechocystis sp. PCC 6803: development of a novel succinate-producing strain. Plant Cell Physiol. 59, 72–81. https://doi.org/10.1093/pcp/pcx162.

Tan, C.H., Lee, K.W.K., Burmølle, M., Kjelleberg, S., Rice, S.A., 2017. All together now: experimental multispecies biofilm model systems. Environ. Microbiol. 19, 42–53. https://doi.org/10.1111/1462-2920.13594.

Tapia, H., Koshland, D.E., 2014. Trehalose is a versatile and long-lived chaperone for desiccation tolerance. Curr. Biol. 24, 2758–2766. https://doi.org/10.1016/j.cub.2014.10.005.

Thomas, Andrew D., Elliott, David R., Hardcastle, David, Strong, Craig L., Bullard, Joanna, Webster, Richard, Lan, Shubin, 2022. Soil biocrusts affect metabolic response to hydration on dunes in West Queensland, Australia. Geoderma 405, 115464. https://doi.org/10.1016/j.geoderma.2021.115464.

Timoner, X., Acuña, V., Von Schiller, D., Sabater, S., 2012. Functional responses of stream biofilms to flow cessation, desiccation and rewetting. Freshw. Biol. 57, 1565–1578. https://doi.org/10.1111/j.1365-2427.2012.02818.x.

Tuel, A., Eltahir, E.a.B., 2020. Why is the Mediterranean a climate change hot spot? J. Clim. 33, 5829–5843. https://doi.org/10.1175/JCLI-D-19-0910.1.

UNI EN 1925, 2000. Metodi di prova per pietre naturali - Determinazione del coefficiente di assorbimento d'acqua per capillarità.

Viles, H.A., Cutler, N.A., 2012. Global environmental change and the biology of heritage structures. Glob. Chang. Biol. 18, 2406–2418. https://doi.org/10.1111/j.1365-2486.2012.02713.x.

Villa, F., Cappitelli, F., 2019. The ecology of subaerial biofilms in dry and inhospitable terrestrial environments. Microorganisms 7, 380. https://doi.org/10.3390/microorganisms7100380.

Villa, F., Remelli, W., Forlani, F., Gambino, M., Landini, P., Cappitelli, F., 2012. Effects of chronic sub-lethal oxidative stress on biofilm formation by Azotobacter vinelandii. Biofouling 28, 823–833. https://doi.org/10.1080/08927014.2012.715285.

Villa, F., Pitts, B., Lauchnor, E., Cappitelli, F., Stewart, P.S., 2015. Development of a laboratory model of a phototroph-heterotroph mixed-species biofilm at the stone/air interface. Front. Microbiol. 6. https://doi.org/10.3389/fmicb.2015.01251.

Vuoristo, K.S., Mars, A.E., Sangra, J.V., Springer, J., Eggink, G., Sanders, J.P.M., Weusthuis, R.A., 2015. Metabolic engineering of the mixed-acid fermentation pathway of Escherichia coli for anaerobic production of glutamate and itaconate. AMB Express 5, 61. https://doi.org/10.1186/s13568-015-0147-y.

Warscheid, T., Leisen, H., 2011. Microbiological studies on stone deterioration and development of conservation measures at Angkor Wat. Biocolonization of Stone: Control, Preventive Methods, pp. 1–18.

Xia, J., Sinelnikov, I.V., Han, B., Wishart, D.S., 2015. MetaboAnalyst 3.0–making metabolomics more meaningful. Nucleic Acids Res. 43, W251–W257. https://doi.org/10.1093/nar/gkv380.

Yang, Y., Li, M., Zheng, X., Ma, H., Nerenberg, R., Chai, H., 2022. Extracellular DNA plays a key role in the structural stability of sulfide-based denitrifying biofilms. Sci. Total Environ. 838, 155822. https://doi.org/10.1016/j.scitotenv.2022.155822.

Zhang, Q., Yan, T., 2012. Correlation of intracellular trehalose concentration with desiccation resistance of soil Escherichia coli populations. Appl. Environ. Microbiol. 78, 7407–7413. https://doi.org/10.1128/AEM.01904-12.

Zhang, J.-Y., Hess, W.R., Zhang, C.-C., 2022. "Life is short, and art is long": RNA degradation in cyanobacteria and model bacteria. mLife 1, 21–39. https://doi.org/10.1002/mlf2.12015.